ChemPubSoc Europe

DOI: 10.1002/chem.201801714

CHEMISTRY A European Journal Full Paper

Polymerization |*Hot Paper*|

Intra- and Interparticle Heterogeneities in Solid Activators for Single-Site Olefin Polymerization Catalysis as Revealed by Micro-Spectroscopy

Marjolein E. Z. Velthoen, Johannes D. Meeldijk, Florian Meirer, and Bert M. Weckhuysen*[a]

Abstract: Methylaluminoxane (MAO) is an activator for single-site olefin polymerization catalysts. Structural characterization of MAO, and in particular the influence of its heterogenization on a silica support, is pivotal for the understanding and optimization of this versatile co-catalyst. In this work, we demonstrate that by varying the MAO loading on a silica support, we can tune the single particle characteristics in terms of MAO distribution and consequent activity. At low MAO loading we reveal two possible intraparticle MAO distributions: a homogeneous and an Al-shell type distribution. With increasing MAO loading, the interparticle MAO distribution becomes more homogeneous. Acidity probing measurements on the single particle level explain how a different intraparticle MAO distribution results in a different activity in metallocene activation. Al-shell particles contain remaining silanol groups and a negligible amount of acid sites and are, therefore, considered inactive for metallocene activation. Only the solid activator particles with a homogeneous intraparticle MAO distribution contain a sufficient number of acid sites, capable of activating the deposited metallocenes.

Introduction

The impact of supported single-site olefin polymerization catalysts relies on the presence of well-defined and highly selective active sites. Moreover, the synergistic advantage of employing such highly active and selective catalysts in the framework of a continuous high-throughput gas- and slurry phase process has resulted in significant progressive industrial interest over the last decade.[1–3] A typical single-site olefin polymerization catalyst comprises a group 4 transition metal in complex with cyclopentadienyl-derived ligands, specifically tailored to selectively produce the desired polymeric material. Prior to catalytic reaction, these metallocenes require interaction with aluminum alkyls to give rise to the cationic species, active in olefin polymerization.[2] Methylaluminoxane (MAO), produced via controlled hydrolysis of trimethylaluminum (TMA), is known to be the most frequently employed activator, but is required in excessive amounts.[4]

Rational catalyst design, including optimized support/activator/metallocene ratios, calls for detailed identification of the surface species actively involved in metallocene activation and olefin polymerization. The inherent structural heterogeneity in solid catalysts, in addition to relatively low concentrations of metallocenes compared to the yet debatable MAO structure, makes this a non-trivial task. Moreover, the heterogenization of the MAO/metallocene olefin polymerization catalyst and the subsequent control of its physicochemical properties is a challenging process.[5] Parameters, such as catalyst structure, co-catalyst loading, synthesis conditions, pre-treatments, and choice of oxidic support including its physical properties, strongly influence the overall structure and, consequently, the catalytic activity of the final supported single-site catalyst material. They are all very important and have to be taken into account when comparing results on different systems stemming from different research groups.[6–10]

Recently, we have reported the influence of MAO loading on metallocene activity in the silica-supported single-site olefin polymerization catalyst.[11] With increasing MAO loading, the amount of weak Lewis acid sites in the solid activator (MAO/SiO_2) increases, showing a linear correlation with olefin polymerization activity. These weak Lewis acid sites in supported MAO materials are therefore assigned to the active species in metallocene activation. In accordance with literature, the weak Lewis acid sites are considered the origin of mobile $AlMe_2^+$ groups, which have often been ascribed to the active species for metallocene activation.[12–16] Remaining silanol groups on the silica support after MAO impregnation, on the other hand, are found to deactivate metallocenes upon interaction.[17–20] TMA, inherently present in commercial MAO solutions, is the responsible species capable of quenching these silanol groups during the synthesis of the solid activators.[2] A minimum MAO

[a] M. E. Z. Velthoen, J. D. Meeldijk, Dr. F. Meirer, Prof. Dr. B. M. Weckhuysen
Debye Institute for Nanomaterials Science
Utrecht University
Universiteitsweg 99, 3584 CG Utrecht (The Netherlands)
E-mail: B.M.Weckhuysen@uu.nl

Supporting information and the ORCID identification number(s) for the author(s) of this article can be found under:
https://doi.org/10.1002/chem.201801714.

Part of the Special Issue for the 7th EuCheMS Chemistry Congress comprising of contributions from selected speakers and conveners. To view the complete issue, visit Issue 46.

loading is, therefore, required to scavenge all silanol groups on the support surface.[11]

In this work, we have extended our characterization studies towards single activator particle analysis. To that end, we have studied the influence of the MAO loading on the creation of active sites in the MAO (weak Lewis acid sites) for metallocene activation and on the level of silanol scavenging within single solid activator particles, employing infrared micro-spectroscopy in combination with pyridine as a probe molecule for acid sites. The results were explained and rationalized by studying possible intraparticle MAO distributions over the silica support with scanning transmission electron microscopy (STEM) in combination with energy-dispersive X-ray (EDX) spectroscopy. Furthermore, the MAO distribution on the single activator particle was extrapolated to a statistical description of the interparticle MAO distribution, using scanning electron microscopy (SEM)-EDX. Finally, N_2-physisorption was employed to study the distribution of MAO over the accessible pores in the silica carrier.

Based on these results, new insights in the role of solid activators for single-site olefin polymerization catalyst activation were obtained. The single particle characterization approach demonstrates in particular that the necessity of using excessive amounts of MAO in the supported metallocene olefin polymerization system does not merely rely on the creation of more active sites capable of activating metallocenes, as is often assumed. Instead, the MAO loading greatly influences its distribution over the silica surface on the single particle level, which appears to be extremely important for the optimization of the silica/MAO/metallocene olefin polymerization catalyst. Bulk-averaged characterization tools are incapable of showing this, hence, demonstrating the added value of extensive analysis on the single particle level.

Results and Discussion

Table 1 a summarizes the chemical composition of the studied supported MAO activators, further denoted as Si-(n)Al, where n indicates the MAO loading (wt% Al) on the silica support. In previous work, these solid activators were utilized as solid activator supports for a zirconocene precursor (*bis*(1-methyl-3-butylcyclopentadienyl) zirconium dichloride), resulting in active catalysts further labeled as Zr/Si-(n)Al, for the ethylene-1-hexene olefin co-polymerization reaction. The catalytic activity for the corresponding catalysts, expressed in kg polyethylene produced per mmol zirconium per hour, is indicated in Table 1 b.[11] A reference catalyst, containing only the parent silica impregnated with the catalyst precursor and denoted as Zr/Si-0Al, was not active in the olefin co-polymerization reaction, indicating the necessity of the MAO activator. In what follows, we present the results obtained with FT-IR micro-spectroscopy in combination with pyridine as probe molecule for acid sites. We will then proceed with the results from STEM-EDX, SEM-EDX, and N_2 physisorption, revealing intra- and interparticle heterogeneities for this solid activator system.

Table 1. Elemental composition of the supported activators (a) and corresponding metallocene-based catalysts (b) including the catalytic activity in the ethylene-1-hexene olefin co-polymerization reaction.

a) Solid activators (MAO/SiO_2)		b) Catalysts ($Zr/MAO/SiO_2$)			
Sample name	Al (wt%)	Sample name	Zr (wt%)	Al/Zr (molar ratio)	Activities (kgPE/mmol Zr·h)
Si-0Al	0	Zr/ Si-0Al	0.26	–	–
Si-6Al	6.3	Zr/ Si-6Al	0.42	051	15.5
Si-9Al	8.9	Zr/ Si-9Al	0.39	077	24.7
Si-12Al	12.3	Zr/ Si-12Al	0.42	098	52.5
Si-14Al	14.0	Zr/ Si-14Al	0.36	131	65.7
Si-17Al	16.9	Zr/ Si-17Al	0.42	132	95.2

Interparticle distribution of active sites in solid activators

In our previous work, we have reported that an increase in MAO loading leads to the creation of more weak Lewis acid sites in the supported activator.[11] These weak Lewis acid sites (W-LAS) are the main responsible species for metallocene activation for olefin polymerization catalysis. The presence of silanol groups on the silica support, on the other hand, was reported to cause the deactivation of metallocenes. They are, therefore, undesirable in the solid activators. Here, we have investigated whether the loading of MAO influences the interparticle distribution of metallocene activating (W-LAS) and deactivating (silanol) species. To that end, the acidic properties of single activator particles were investigated with FT-IR micro-spectroscopy in combination with pyridine as a probe molecule for acid sites. We determined the acidic properties of 20 individual activator particles per MAO/SiO_2 sample. Samples were loaded in a Linkam cell in a N_2 glovebox and transported to the microscope, where the solid activator particles were subjected to a dry N_2 flow. A spectrum for each activator particle was recorded, prior to pyridine adsorption for 30 min, after which a second spectrum was collected. After pyridine adsorption the sample was heated to 200 °C to remove physisorbed pyridine. The recorded spectra after this desorption treatment indicate pyridine adsorbed on acid sites. Figure 1 illustrates typical FT-IR spectra before (black), after pyridine adsorption at RT (red), and after desorption at 200 °C (blue) for single solid activator particles, taking the Si-6Al and Si-17Al materials as a

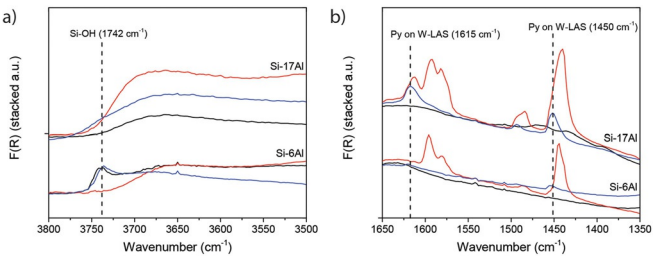

Figure 1. FT-IR spectra depicting the ν-OH region (a) and the pyridine ring vibrational region (b) for two single solid activator particles of Si-6Al and Si-17Al, respectively. In black, the spectrum before pyridine adsorption is plotted, the red spectrum was recorded after pyridine adsorption at RT, and the blue spectrum shows the spectrum after desorption at 200 °C.

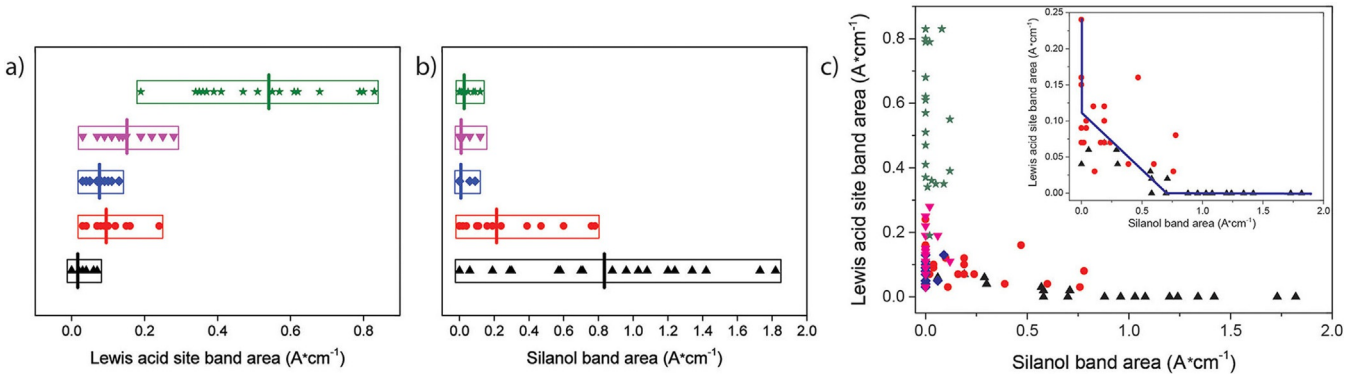

Figure 2. Lewis acid site (a) and silanol (b) band areas for the individual solid activator particles with increasing MAO loading: Si-6Al (black), Si-9Al (red), Si-12Al (blue), Si-14Al (purple), and Si-17Al (green). The boxes represent the total distribution range per sample and the average value is indicated with a vertical line. In (c), the Lewis acid site band areas are plotted versus the silanol band areas. The insert depicts a zoom on solid activators with significant silanol band areas: Si-6Al (black) and Si-9Al (red). The blue line is drawn to guide the eye.

showcase. The ν-OH region (3800-3500 cm^{-1}), shown in Figure 1a, demonstrates whether the particle contains any silanol groups, indicated by a band at 3472 cm^{-1}. The disappearance of this band after pyridine adsorption at RT demonstrates the interaction between pyridine and silanol groups through hydrogen bonding. At 200 °C this pyridine is desorbed, as indicated by the returning band at 3742 cm^{-1} in the blue spectrum. Figure 1b shows the fingerprint region of the pyridine ring vibrations (1650–1350 cm^{-1}). Previously, we have demonstrated the MAO/SiO_2 solid activators to have a concentration of weak Lewis acid sites that linearly correlates with MAO loading.[11] This weak Lewis acid site is observed in pyridine FT-IR spectroscopy via bands at 1615 and 1450 cm^{-1}. Other bands in this region characterize pyridine when adsorbed on non-acidic silanol groups.[21,22] Upon temperature treatment at 200 °C, only the bands ascribed to pyridine adsorbed on acid sites are still present. In summary, Figure 1 shows the pyridine FT-IR spectra of a solid activator particle containing a low amount of silanol groups and a significant amount of weak Lewis acid sites (found in sample Si-17Al) and a solid activator particle containing a high amount of silanol groups with a negligible amount of acid sites (found in sample Si-6Al). These two sets of spectra, therefore, represent a particle that is assumed active (Si-17Al) and inactive (Si-6Al), respectively, in the activation of metallocenes for olefin polymerization.

For every sample, that is, the Si-(n)Al) materials with $n=6$–17, pyridine FT-IR spectra of 20 solid activator particles were collected. After background subtraction, the total band areas under the resulting bands at 3742 and 1614 cm^{-1} were integrated. These band positions were selected based on their conclusive band assignments, that is, there is no possible band overlap with other surface species. The integrated band areas were then taken as a measure of the amount of silanol groups and weak Lewis acid sites in each particle, respectively. The spectra were taken in reflectance mode over an aperture of 50×50 μm. Assuming similar probed volume and similar reflective properties for the samples with different MAO loadings, the integrated band areas can be taken as a measure of quantity. Figures 2a and 2b show the interparticle distribution in terms of amount of acid sites and amount of silanol groups, respectively. The vertical bars indicate the average value over 20 activator particles within the MAO/SiO_2 sample. It is observed that with increasing MAO loading, the particles contain on average more Lewis acid sites and less silanol groups. Moreover, solid activators with a MAO loading of 12 wt% Al and higher, do not contain particles with silanol groups. These observations are all in correspondence with the previous pyridine FT-IR studies on the bulk material. In the Supporting Information, the FT-IR spectra collected before and after pyridine adsorption for all particles can be found, including histograms on the silanol and pyridine on Lewis acid site band areas per solid activator (Figure 1).

Figure 2c demonstrates the correlation between the amount of silanol groups and Lewis acid sites within individual solid activator particles. It appears that a particle containing silanol groups does not contain Lewis acid sites and vice versa. This would imply that a solid activator particle is either an active or inactive particle for metallocene activation. A closer examination of the data set from the samples with a significant amount of silanol groups (i.e. Si-6Al and Si-9Al in the insert) reveals that only particles with a low amount of silanol groups (band area <0.5) contain Lewis acid sites. Particles that contain a large amount of silanol groups, on the other hand, have negligible Lewis acid site band areas (1614 cm^{-1}). Furthermore, Figure 2 reveals that for samples without silanol groups (i.e. Si-12Al, Si-14Al, and Si-17Al) the average amount of Lewis acid sites correlates with the MAO loading, but the interparticle distribution of also becomes more heterogeneous. Sample Si-17Al indeed shows the largest spread in amount of Lewis acid sites per individual particle. The single particle pyridine FT-IR therefore demonstrates an interparticle dichotomy in which an individual solid activator particle is either active (a Lewis acidic particle) or inactive (silanol groups) in metallocene activation.

Intraparticle heterogeneity in MAO distribution over the silica support

In order to understand the observed interparticle dichotomy of active versus inactive activator particles, the distribution of MAO over the silica support within a single silica particle was studied with scanning transmission electron microscopy (STEM) in combination with energy dispersive X-ray (EDX) spectroscopy. To that end, ultra-microtomed slices (70 nm thick) of supported activator particles were prepared, allowing for the determination of the MAO distribution throughout the entire silica particle, instead of merely observing the external particle surface. The measurements were performed for all five supported activators with increasing MAO loading (6–17 wt% Al) in order to study the influence of MAO loading on its possible intraparticle distributions. Figure 3 depicts the respective STEM micrographs, the Si (SiO_2) and Al (MAO) elemental maps, and the overlay of the Si and Al elemental maps for one particle within the solid activator with the lowest (Si-6Al, Figure 3a) and highest (Si-17Al, Figure 3b) MAO loading. Similar to the FT-IR micro-spectroscopy measurements, approximately 20 solid activator particles were studied per MAO/SiO_2 sample and for each solid activator particle, the Al/Si elemental map can be found in the Supporting Information (Figures S2–6). Furthermore, for each solid activator particle, the EDX spectra at both the inside of the particle (bulk) and at the edge (thickness approximately 0.5 μm) were quantified. In these quantifications the accumulated Si and Al count was considered 100%. The resulting atomic Al/Si ratios were then deduced from the EDX spectra. The bulk and edge areas were manually selected regions in the micrographs and are indicated in the Supporting Information.

Two types of solid activator particles could be distinguished in the set of materials under study; the so-called "aluminum-shell" distribution type, in which the MAO (aluminum, red) is only deposited on the edge of the silica particle (blue), is shown in Figure 3a. The second type is referred to as the "homogeneous" MAO/silica particle, in which the MAO is homogeneously distributed over the silica particle (Figure 3b). We define the MAO distribution to be homogeneous when the Al/Si ratio in the bulk of the particle resembles the Al/Si ratio at the edge (outer 0.5 μm) of the particle, that is, when the ratio $Edge_{Al/Si}$:$Bulk_{Al/Si}$ was found smaller than 1.2. When the Al/Si ratio is significantly higher at the edge (i.e. $Edge_{Al/Si}$:$Bulk_{Al/Si}$ >1.2) the solid activator particle is considered to have an aluminum shell type distribution. Table 2 shows the number of particles for each type of solid activator particle per sample and indicates that with increasing MAO loading, the amount of aluminum-shell particles decreases in each sample, while the number of homogeneous particles increases. The solid activators Si-6Al and Si-9Al predominantly contain particles where MAO is found on the external surface of the silica particle. The highest loaded solid activator (i.e. Si-17Al), on the other hand, only contains homogeneous particles.

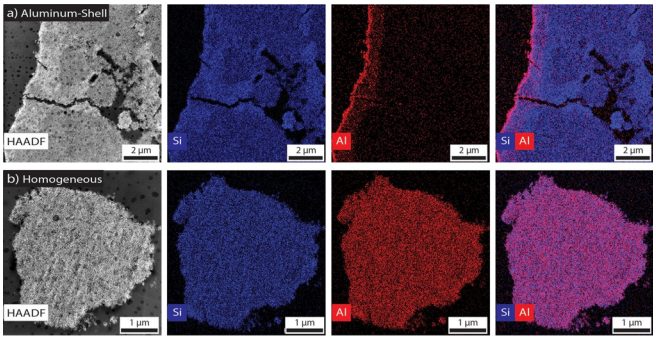

Figure 3. STEM micrographs with corresponding Si (blue) and Al (red) elemental maps, as determined with EDX spectroscopy. Two typical intraparticle aluminum distributions illustrating the studied supported activators are depicted: Aluminum-Shell (a, Si-6Al) and Homogeneous (b, Si-17Al).

In summary, it has now been established that with increasing MAO loading, there is a gain in activator particles with a homogeneous intraparticle MAO distribution, in parallel with a gain in active, Lewis acidic, activator particles. It is, therefore, proposed that only particles with a homogeneous intraparticle MAO distribution can be active in the activation of metallocene precursors, leading to catalytic olefin polymerization activity.

The supporting of MAO on a silica support is assumed to be aided by trimethylaluminum (TMA).[2,5,23] TMA reacts and binds on the silanol groups on the surface and the MAO is, subsequently, anchored on the surface TMA groups. The STEM-EDX results in Figure 3 display the two types of intraparticle MAO distribution, namely the Al-shell and the homogeneous distribution. It can be argued that during synthesis, TMA reacts with external silanol groups first and is then transported inside the particle. Thus, in case of a shortage of TMA, the silanol groups in the pores remain unreacted. As a consequence, the MAO can only anchor on the external surface of the silica particle, resulting in an Al-shell type distribution. In the previous section, we have demonstrated that in solid activators Si-6Al and Si-9Al a significant amount of activator particles still contain silanol groups on the surface after interaction with the commercial MAO solution.[11] This indicates a shortage of TMA to interact with all silanol groups. The clear presence of Al-shell type particles in these solid activators can indeed suggest an absence of aluminum alkyls in the bulk of the particles, explaining the presence of remaining silanol groups in these particular activator particles.

This, however, does not explain the observation that solid activator particles with an Al-shell type distribution are also observed in samples without silanol groups, that is, Si-12Al and Si-14Al (indicated in Figure 2b, previous work,[11] and Table 2).

Table 2. Number of particles with an aluminum shell or with a homogeneous distribution of MAO over the silica support.

Solid activator	Measured particles	Aluminum shell ($edge_{Al/Si}$:$bulk_{Al/Si}$ >1.2)	Homogeneous ($edge_{Al/Si}$:$bulk_{Al/Si}$ <1.2)
Si-6Al	20	16	4
Si-9Al	20	15	5
Si-12Al	19	7	12
Si-14Al	19	8	11
Si-17Al	19	0	19

Interestingly, we can distinguish two subcategories within the category of aluminum shell type distributions: There are "empty" silica particles with a thin MAO layer on the external surface, but also activator particles with a homogeneous MAO distribution inside the bulk of the particle with an additional layer of MAO on the external surface. The EDX elemental maps for all particles in the Figures S2–6 give a clear visual representation of this difference. Both types of solid activator particles, however, have a $Edge_{Al/Si}$:$Bulk_{Al/Si} > 1.2$, placing them in the Al-Shell category. The former distribution leads to a ratio above 2, whereas the latter has a ratio between 1.2 and 2.

In the case that there was enough TMA to quench all silanol groups, the MAO is free adsorb throughout the entire silica particle. The formation of Al-Shell type distributions with a significant amount of MAO on the internal silica surface is suggested to be caused by not enough MAO to form MAO layers with the maximum thickness. MAO can strongly adsorb in several layers on the surface and, apparently, the external surface is fully saturated before the inner surface is completely saturated. This would then result in $Edge_{Al/Si}$:$Bulk_{Al/Si}$ ratios between 1.2 and 4. On the other hand, there are Al-shell particles with an almost MAO depleted inner silica surface and only MAO on the external surface have $Edge_{Al/Si}$:$Bulk_{Al/Si}$ ratios in the range of 10–50, as observed in solid activator Si-6Al.

The average $Edge_{Al/Si}$:$Bulk_{Al/Si}$ ratio and standard deviation as a function of MAO loading, as shown in Table 3, indeed shows that solid activators Si-12Al and Si-14Al do not contain empty silica particles anymore, but merely do not contain enough MAO to saturate all available surface area. As a result, there is still a higher Al concentration at the edge than in the bulk of the particle. The highest loaded sample, Si-17Al, apparently does contain enough MAO to spread it homogeneously through the particle, resulting in an $Edge_{Al/Si}$:$Bulk_{Al/Si}$ ratio of approximately 1 (0.93 ± 0.10). Table 3 also provides an indication of how the intraparticle heterogeneity decreases with increasing MAO loading. For Si-6Al, the MAO is often merely situated on the external surface and almost absent in the bulk of the particle. This is clearly expressed by a high average $Edge_{Al/Si}$:$Bulk_{Al/Si}$ ratio. The standard deviation (14.92) also demonstrates the large variety between particles. With increasing MAO loading, the average $Edge_{Al/Si}$:$Bulk_{Al/Si}$ ratio approaches 1 (i.e. 1.75 for Si-12Al and 1.27 for Si-14Al), indicating a more homogeneous intraparticle MAO distribution. The significantly lower standard deviation also demonstrates the decreasing interparticle heterogeneity. The particles of solid activator Si-17Al all show a homogeneous intra- and interparticle distribution.

Table 3. Average $Edge_{Al/Si}$:$Bulk_{Al/Si}$ ratio and standard deviation for the studied supported activators. Tables S1–S5 (Supporting Information) show the separately obtained bulk and edge Al/Si ratios for all activator particles.

Solid activator	Average $edge_{Al/Si}$:$bulk_{Al/Si}$	Standard deviation
Si-6Al	9.80	14.92
Si-9Al	3.12	5.32
Si-12Al	1.75	1.20
Si-14Al	1.27	0.35
Si-17Al	0.93	0.10

The presence of Al-shell MAO distributions has been reported in literature before based on SEM-EDX measurements.[5] Such distributions were then ascribed to poor mixing of the silica/MAO slurry, rapid addition of MAO to the silica slurry, or too low MAO concentrations.[5,24] As a result, metallocenes were activated on the external surface of the solid activator, leading to hollow polymer particles with a low bulk density.[25,26] Previously, we showed that catalysts with low MAO loading indeed yield polymers with low bulk density, which we ascribed to metallocene leaching from the activator surface.[11] This could, however, now also be ascribed to the presence of Al-shell particles, as demonstrated in this work, suggesting that some particles contain both silanol groups as well as Lewis active sites. Figure 2c indeed confirms that the possibility of having a particle with silanol groups in the bulk and active sites in the shell cannot be excluded. A SEM study of the formed polymers was outside the scope of this work, so we cannot confirm the formation of hollow polymer particles. It is, therefore, proposed that a combination of both factors (polymerization on the external activator surface and metallocene leaching) leads to poor quality polymer.

Interparticle heterogeneity in MAO distribution over the silica support

The statistical description of interparticle heterogeneity was extrapolated to a significantly larger dataset (approximately 500 particles per solid activator), employing scanning electron microscopy (SEM) in combination with energy dispersive X-ray (EDX) spectroscopy elemental mapping (Si and Al). Figure 4 depicts the respective SEM images, the Al and Si elemental maps, and the Al/Si overlay for all studied solid activators. Regarding the distribution of aluminum, and therefore of MAO, it can be observed that the distribution homogenizes with increasing loading. The solid activator Si-6Al shows an aluminum coverage of approximately 50%, which increases with increasing MAO loading until samples Si-14Al and Si-17Al, which show a full coverage of aluminum. It is important to note that the X-ray penetration depth in SEM-EDX is approximately a micrometer. This means that a small MAO shell of 0.5 μm on the silica external surface, as observed for the aluminum-shell type particles (Figure 3a), will not be detected and the particle is (mis)-classified as an empty silica particle. The overlay of all elemental maps (Figure 4, right) is the most informative for a complete overview of the coverage of SiO_2 particles. The color red is indicative of the presence of both Si and Al, blue for only Si, and green for only Al. If the particles do not show any color, it means that X-rays from this location were unable to reach the EDX detector. This effect is visible in every SEM image via a "shadow" on the top right of each particle.

The solid activators Si-14Al and Si-17Al mainly consist of particles with a homogeneous MAO distribution, as indicated by the red color. This is in correspondence with the results from STEM-EDX, showing mainly homogeneous intraparticle MAO distributions with a $Edge_{Al/Si}$:$Bulk_{Al/Si} < 1.2$. Interestingly, the

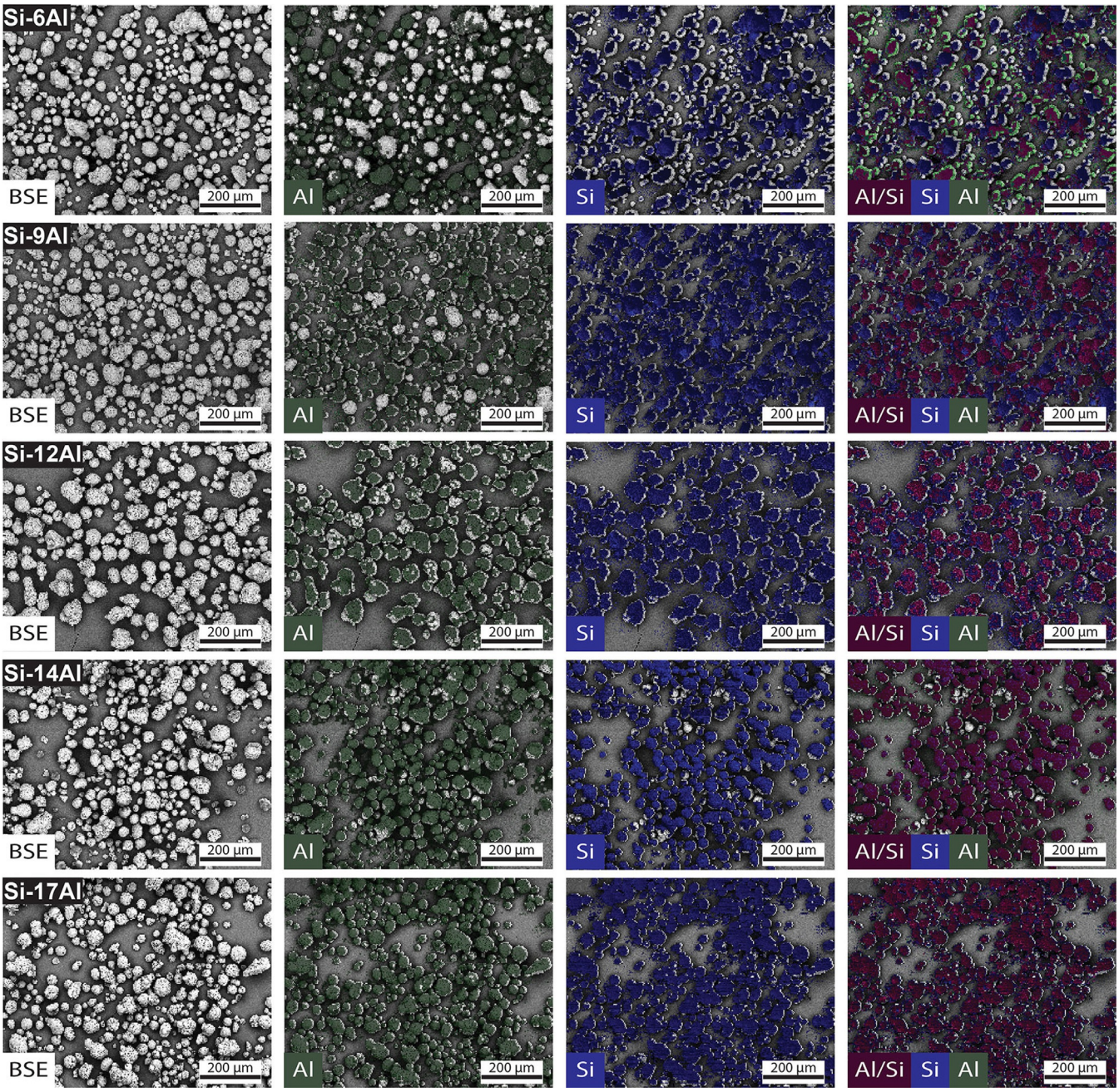

Figure 4. SEM images with corresponding Al (green), Si (blue), and Al/Si (red) elemental maps, as determined with EDX spectroscopy for the studied solid activators with increasing MAO loading (6–17 wt% Al).

solid activators Si-12Al and Si-9Al contain a relatively lower loading of aluminum and exhibit two types of particles: homogeneous distributions and particles with only partial coverage of aluminum (MAO). The latter show both blue and red parts within one particle. The solid activator Si-6Al has the most interesting distribution with three types of particles: plain SiO_2 (blue), partial Al coverage (blue and red), and particles completely covered with MAO, including an extra layer of aluminum on top of the SiO_2 particle (red and green). Si-9Al and Si-12Al also contain a few particles of this last category, as indicated by the green color in their respective images. The combined Al/Si maps therefore give a more specific description of the interparticle heterogeneity compared to the Al maps.

The EDX elemental maps, as represented in Figure 4, were employed to express the observed interparticle heterogeneity in a numerical manner. Within each measured particle, the average aluminum intensity over all pixels within one particle was plotted versus the average silicon intensity (see also Figure S7). This resulted in the scatterplots depicted in Figure 5, in which each data point represents the correlation between the amount of silicon and aluminum within a single particle in the respective solid activator. Figure 5 also provides the Pearson correlation coefficient between the Si and Al intensity for each

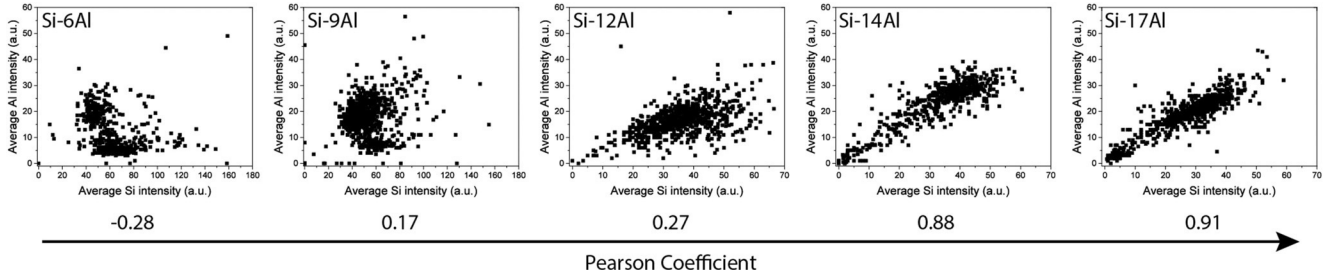

Figure 5. Scatterplots for the studied solid activators Si-(n)Al, showing the average Al intensity versus average Si intensity per individual activator particle. The Pearson correlation coefficient represents the interparticle heterogeneity for each solid activator.

solid activator and represents the degree of interparticle heterogeneity in terms of MAO distribution over the silica particles. A Pearson correlation coefficient close to 1 (or −1) is indicative of a strong positive (or negative) spatial correlation, that is, interparticle homogeneity, whereas a correlation coefficient close to 0 signifies no spatial correlation and, therefore, a clear interparticle heterogeneity. With a Pearson correlation coefficient steadily increasing from −0.28 (slightly negative Al Si correlation) for Si-6Al via 0.17 for Si-9Al (no significant correlation) and 0.27 for Si-12Al (slightly positive correlation) to a significantly positive Al Si correlation for Si-14Al (0.88) and Si-17Al (0.91), Figure 5 clearly shows that the interparticle heterogeneity correlates inversely proportional with the MAO loading of the solid activators. Interestingly, the trend for Pearson correlation coefficients with increasing MAO loading seems to indicate a change in the correlation from negative to strongly positive with a minimum (perfectly no correlation) between Si-6Al and Si-9Al. This supports the conclusion that at low MAO loadings, TMA only reacts on the external silica surface, resulting in the anchoring of MAO only on top of the silica particle. Hence, in the SEM-EDX results, there is either a high Al and low Si intensity or vice versa, resulting in a negative Pearson correlation coefficient. Here, it has to be noted that, although the Pearson correlation coefficients for Si-6Al, Si-9Al, and Si-12Al are rather low, the correlation plots clearly support the above-mentioned conclusion.

In this work we have demonstrated a new approach to accurately determine interparticle heterogeneities in solid catalysts. The key to a reliable interparticle description relies on having a large amount of screened particles within one sample to prevent the description of mere outliers. The problem with large-scale particle screening, however, is the lack of details on the single particle level. We propose that an extensive bulk analysis in combination with an extensive study on a small amount of single particles provides a nearly complete picture of the chemistry within a catalytic system. This knowledge can then be used to chemically rationalize the results obtained from large-scale single particle screening. Scheme 1 illustrates this method. In this work, we have used SEM-EDX spectroscopy to screen many particles simultaneously to unravel interparticle heterogeneities. The chemical interpretation of the interparticle MAO distribution is obtained from detailed analysis of both the bulk material and single particles. Bulk analysis from previous work provided a good overview of the presence and ratio

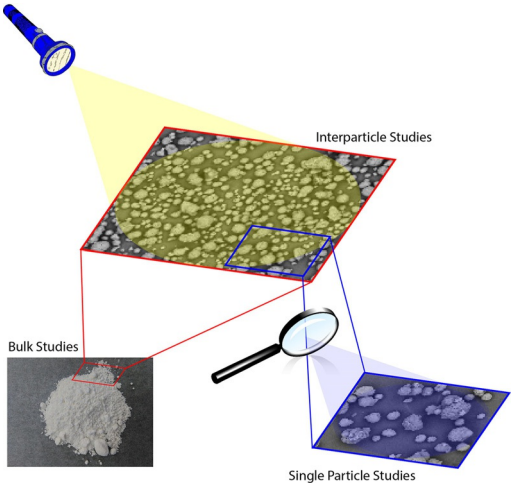

Scheme 1. Method to accurately determine interparticle heterogeneities: A multiple length scale approach of both bulk and single particle studies allows for the interpretation of large scale single particle screening.

of different species and trends in concentration as a result of changed synthesis parameters.[11] The results from the bulk study, therefore, provided a well-founded hypothesis for the interparticle study. A single particle study, on the other hand, reveals chemical intraparticle heterogeneities. In this work, we have employed different methods to study single activator particles, namely STEM–EDX spectroscopy and pyridine FT-IR micro-spectroscopy. The results gave very detailed insights in the chemistry within a single activator particle and were pivotal in explaining the interparticle heterogeneities, as determined with SEM–EDX.

The distribution of MAO over the silica pore network

The two possible intraparticle MAO distributions over the porous silica network and the resulting interparticle heterogeneity in terms of distribution of active Lewis acid sites raise questions about how the silica pore network changes upon impregnation of MAO. To that end, we employed N_2 physisorption to study the influence of MAO loading on the porous properties of the solid activators. In the Supporting Information (Figure S8), the N_2 adsorption and desorption isotherms can be found. Figure 6 shows the accumulated pore volume

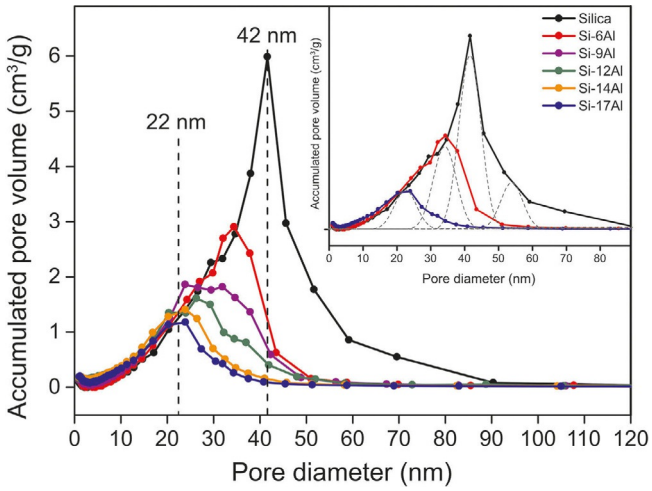

Figure 6. N_2 physisorption results, showing the accumulated pore volume ($cm^3 g^{-1}$) plotted vs. the pore diameter (nm) for the silica support and corresponding five solid activator samples with increasing MAO loading. The insert shows only the parent silica and the solid activator with the lowest (Si-6Al) and highest (Si-17Al) MAO loading. As a guide to the eye, normal distribution functions are drawn to indicate the multimodal pore size distributions in the samples.

($cm^3 g^{-1}$) as a function of pore diameter (nm) for the silica support and five solid activators with increasing MAO loading. The parent silica material mainly contains 42 nm diameter pores. These pores become smaller with increasing MAO loading, but reach a plateau at 22 nm diameter. Moreover, the parent silica presents a multimodal pore size distribution with pore sizes ranging from 10 to 80 nm in diameter, whereas this distribution becomes narrower upon MAO impregnation. The large pores are filled preferentially, as can be derived from the pore size distributions in Figure 6. A decreasing pore size from 42 to 22 nm in diameter suggests MAO layers in the silica pores with a maximum thickness of 10 nm. Indeed, increasing the MAO loading from 12 to 17 wt% Al does not lead to a closer filling of the pores, as indicated by the plateau at 22 nm. Instead, other larger pores are consumed until the 22 nm diameter is reached again, indicated by a decreasing tail at 35 nm. The insert in Figure 6 displays how the multimodal pore size distribution, still present in Si-6Al, resolves to a narrow distribution at 22 nm for Si-17Al.

These results confirm the conclusions from the STEM-EDX and SEM-EDX results. MAO can strongly adsorb in several layers on the surface and, apparently, the external surface is fully saturated before the inner surface is completely saturated. When all available silica surface is completely saturated, that is, when the maximum layer of 10 nm is achieved, the pore size distribution is centered at 22 nm. In that case (Si-17Al) we have a completely homogeneous intraparticle MAO distribution with a $Edge_{Al/Si}$:$Bulk_{Al/Si}$ ratio of approximately 1 (0.93 ± 0.10) and a narrow pore size distribution. In the case where lower amounts of MAO are available (Si-12Al and Si-14Al), there is a thinner layer of MAO on the internal silica surface. This results in solid activator particles with an Al-shell type distribution with a $Edge_{Al/Si}$:$Bulk_{Al/Si}$ ratio of approximately 1.5 (1.75 ± 1.20 and 1.27 ± 0.35, respectively) and a wider pore size distribution.

Conclusions

Solid activators (SiO_2/MAO) for metallocene-based olefin polymerization catalysts with increasing MAO loading were characterized on the single particle level. This allowed drawing conclusions about the influence of MAO loading on the intra- and interparticle MAO distribution over the silica support and the resulting catalytic performance, as summarized in Scheme 2.

STEM–EDX measurements provided more insight in the intraparticle heterogeneity at low MAO loadings. It was shown that MAO either distributes homogeneously over the silica particle or anchors on the external silica surface only, creating a so-called Al-shell distribution. The formation of the latter type particles was ascribed to a shortage of TMA in the low loaded samples. MAO strongly adsorbs only on places where TMA has quenched the silanol groups. At low TMA concentrations, only the external surface becomes available for MAO adsorption. With increasing MAO loading, the amount of Al-shell particles

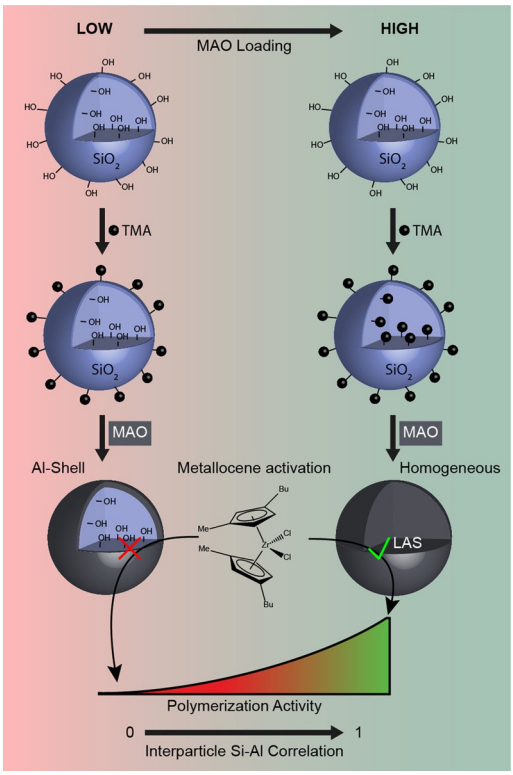

Scheme 2. Schematic of the main conclusions from this work. At low MAO loadings, there is not enough TMA present to quench all present silanol groups. Instead, only the groups on the external surface area interact with the TMA. As a consequence, MAO can only adsorb on the external surface, leading to an Al-Shell type distribution with remaining silanol groups. Upon interaction with these groups, metallocene precursors are deactivated, leading to low polymerization activity. Instead, at high MAO loadings, there is sufficient TMA to react with all available silanol groups, leading to a homogeneous MAO distribution. The Lewis acid sites present in these activator particles are capable of metallocene activation, leading to high olefin polymerization activity.

diminishes and only homogeneous particles remain. FT-IR micro-spectroscopy measurements employing pyridine as a probe molecule, showed how a different intraparticle MAO distribution could lead to a different activity in metallocene activation on the single activator particle level. Particles with remaining silanol groups after MAO impregnation possess a negligible amount of acid sites and are, therefore, inactive for metallocene activation. Only particles with all silanol groups quenched with TMA contain acid sites capable of activating metallocene precursors. The former inactive particles were only found in solid activators Si-6Al and Si-9Al and are, therefore, correlated with particles with an Al-shell MAO distribution with an $Edge_{Al/Si}$:$Bulk_{Al/Si}$ ratio in the range of 10–50, as determined with STEM–EDX. The latter active particles are assigned to particles with a homogeneous MAO distribution or an Al-shell distribution with a $Edge_{Al/Si}$:$Bulk_{Al/Si}$ ratio in the range of 1.2–4. Interestingly, solid activator Si-17Al showed the largest interparticle variation of acid sites, while the MAO is very homogeneously distributed on both an intra- and interparticle level. Since every solid activator particle contains acid sites and no silanol groups, we expect that it will not lead to large differences in the final interparticle distribution of active metallocenes.

The interparticle MAO distribution, as determined with SEM–EDX, demonstrated that the distribution becomes more homogeneous with increasing MAO loading. The correlation coefficient, describing the correlation between Si and Al concentration within one particle, approaches 1 for a solid activator with 14 and 17 wt% Al, whereas for the lowest Al loadings, the Si and Al concentrations seem mainly uncorrelated (or slightly positively, or even negatively, correlated with correlation coefficients of −0.28, 0.17, and 0.27 for a solid activator with 6, 9, and 12 wt% Al, respectively), suggesting significant interparticle heterogeneity.

The N_2 physisorption experiments described in this work support the observation that only at high MAO loading, all pores within the silica particle are filled with MAO, anchored on the silanol groups. At low MAO loading, on the other hand, the MAO is only deposited in the larger and better accessible pores. N_2 physisorption also showed that the average pore size changes from 42 nm in diameter in the parent silica to minimally 22 nm in the solid activator with 17 wt% Al. This indicates that MAO adsorbs in layers with a maximal thickness of 10 nm.

In this work we have demonstrated a new approach to accurately determine interparticle heterogeneities in solid catalysts: Extensive bulk characterization in combination with a detailed study on a small amount of single particles provide a complete picture of the chemistry within a catalytic system. This knowledge can then be used to chemically rationalize the results obtained from large-scale single particle screening.

Experimental Section

Sample preparation: The preparation of the materials was done as described in previous work from our group:[11] Solid activators were prepared according to a synthetic protocol comprising two steps: silica treatment and MAO anchoring. All steps in this procedure were carried out under N_2 atmosphere and all solvents utilized for the synthesis were analytical grade and treated prior to any use in synthesis: Toluene (Fischer Chemical, purity: >5) 99.99% was degassed through dry nitrogen bubbling and dried employing molecular sieves. *N*-pentane (Fischer Chemical, purity: 99%) was dried over calcium hydride. The moisture content was measured by Karl–Fischer titration, giving a content level less or equal to 2 ppm. The 30% MAO solution containing approximately 26.2 wt% MAO and 5.2 wt% TMA was stored in a fridge at 255 K in order to prevent gel formation. All synthetic steps were carried out using standard glovebox techniques and the prepared samples were stored in a N_2 glovebox, inside dark and well-sealed containers. The syntheses yielded a set of samples, consisting of the parent silica and 5 solid activators with increasing MAO loading (Si-(6-17)Al). In this notation, the number preceding the Al indicates the weight loading of Al, with 6 wt% being the lowest and 17 wt% being the highest loading.

A commercial amorphous silica (ES767 from PQ), with a surface area of 276 $m^2 g^{-1}$, a pore volume of 1.56 $cm^3 g^{-1}$, an average pore width of 19.2 nm and a mean particle size of approximately 33 μm diameter, was heated at 423 K for 5 h on a fluidized bed under a dry N_2 flow to remove moisture. In a glass round-bottom flask, an MAO solution was slowly added to a silica/toluene slurry (respective weight ratio of 1:5) under gentle mechanical agitation (precursor: Albemarle 30% MAO solution: 26.2 wt% in toluene, 5.2 wt% residual TMA). Subsequently, the whole mixture was heated at toluene reflux temperature (ca. 384 K) for several hours. The solid was filtered on a frit, washed three times with dry n-pentane followed by a drying treatment under vacuum for 1 h at room temperature. Following this procedure, five solid activators with increasing Al weight loading (6–17 wt%) were prepared.

Sample characterization: The FT-IR micro-spectroscopy measurements with pyridine as a probe molecule were performed on a PerkinElmer Spotlight 400 FT-IR microscope. Samples were prepared in a N_2 glovebox by placing a small amount of solid activator powder on the stage of a Linkam Scientific temperature-controlled cell equipped with a CaF lid. The Linkam stage was connected to an Eheim Professional 3 water cooler and a Linkam TMS 93 heater. In the cell, samples were kept in a N_2 atmosphere and subsequently transported to the microscope, where they were subjected to a N_2 flow of 10 $mL\,min^{-1}$. For each sample, 20 random particles were selected and FT-IR spectra were recorded with an aperture of 50×50 μm. Next, the N_2 flow was sent through a saturator, filled with pyridine, allowing for pyridine adsorption on the solid activator. After 30 min, the flow was adjusted back to pure N_2 and FT-IR spectra were recorded of the same 20 particles again. This was followed by a temperature treatment at 200 °C under N_2 flow to remove physisorbed pyridine, after which FT-IR spectra were recorded of the same 20 particles again.

SEM–EDX measurements were performed on a XL30SFEG (FEI) instrument with a 15 keV beam. Samples were sputtercoated with a 10 nm layer of platinum to increase conductivity. Magnification was always set at 350x and elemental X-ray maps were collected with an EDAX super ultra-thin window detector with a frame size of 256×200 pixels and an integration time of 1000 ms per pixel.

STEM–EDX measurements were performed on a FEI Talos F200X, employing SuperX EDX-detectors. Mapping software was Esprit (Bruker) where the X-ray signal of consecutive fast scans (5 ms per pixel) is accumulated until sufficient signal per pixel is acquired. Different particles were imaged at different magnifications and different pixel resolutions. Samples were embedded in Epofix embedding resin prior to sectioning on an Reichert Jung UltraCut E mi-

crotome to 70 nm sections that were placed on 200 mesh copper grids with carbon coated Pioloform film.

N_2 physisorption was performed at 77 K using a Micromeritics TriStar instrument. The mesopore volumes (the 2–300 nm range) and Barrett–Joyner–Halenda (BJH) pore size distributions of the silica support and solid activators were determined using the adsorption branch of the isotherm with Aerosil 380 as a reference. Samples were prepared in the N_2 glovebox and no additional drying procedures were used.

Acknowledgements

The authors thank Albemarle for financial support. Hugo Peters (Utrecht University, UU) is acknowledged for useful discussions about the statistical treatment of the data. Sander Lambrechts (UU) is thanked for the N_2-physisorption measurements. Furthermore, we thank the Electron Microscopy department of the Utrecht University for facilitating the SEM and STEM measurements.

Conflict of interest

The authors declare no conflict of interest.

Keywords: acidity · heterogeneity · methylaluminoxane · polymerization · spectroscopy

[1] L. Resconi, L. Cavallo, A. Fait, F. Piemontesi, *Chem. Rev.* **2000**, *100*, 1253 – 1345.
[2] J. R. Severn, J. C. Chadwick, R. Duchateau, N. Friederichs, *Chem. Rev.* **2005**, *105*, 4073 – 4147.
[3] S. S. Reddy, S. Sivaram, *Prog. Polym. Sci.* **1995**, *20*, 309 – 367.
[4] H. Sinn, W. Kaminsky, *Adv. Organomet. Chem.* **1980**, *18*, 99 – 149.
[5] J. R. Severn in *Tailor-Made Polym. Via Immobil. Alpha-Olefin Polym. Catal.* (Eds.: J. R. Severn, J. C. Chadwick), Wiley, Weinheim, **2008**, pp. 95 – 138.
[6] M. C. Haag, C. Krug, J. Dupont, G. B. De Galland, J. H. Z. Dos Santos, T. Uozumi, T. Sano, K. Soga, *J. Mol. Catal. A* **2001**, *169*, 275 – 287.
[7] N. L. Krzystowczyk, S. P. Diefenbach, E. A. Burt, US005739368A, **1998**.
[8] D. Bianchini, J. H. Z. Dos Santos, T. Uozumi, T. Sano, *J. Mol. Catal. A* **2002**, *185*, 223 – 235.
[9] T. Sano, H. Hagimoto, S. Sumiya, Y. Naito, Y. Oumi, T. Uozumi, K. Soga, *Microporous Mesoporous Mater.* **2001**, *44 – 45*, 557 – 564.
[10] A. Razavi, G. L. G. Debras, US005719241A, **1998**.
[11] M. E. Z. Velthoen, A. Muñoz-Murillo, A. Bouhmadi, M. Cecius, S. Diefenbach, B. M. Weckhuysen, *Macromolecules* **2018**, *51*, 343 – 355.
[12] F. Ghiotto, C. Pateraki, J. Tanskanen, J. R. Severn, N. Luehmann, A. Kusmin, J. Stellbrink, M. Linnolahti, M. Bochmann, *Organometallics* **2013**, *32*, 3354 – 3362.
[13] L. Luo, S. A. Sangokoya, X. Wu, S. P. Diefenbach, B. Kneale, US8354485B2, **2013**.
[14] J. T. Hirvi, M. Bochmann, J. R. Severn, M. Linnolahti, *ChemPhysChem* **2014**, *15*, 2732 – 2742.
[15] M. S. Kuklin, J. T. Hirvi, M. Bochmann, M. Linnolahti, *Organometallics* **2015**, *34*, 3586 – 3597.
[16] M. Linnolahti, S. Collins, *ChemPhysChem* **2017**, *18*, 3369 – 3374.
[17] B. L. Moroz, N. V. Semikolenova, A. V. Nosov, V. A. Zakharov, S. Nagy, N. J. O'Reilly, *J. Mol. Catal. A Chem.* **1998**, *130*, 121 – 129.
[18] J. Tian, S. Wang, Y. Feng, J. Li, S. Collins, *J. Mol. Catal. A Chem.* **1999**, *144*, 137 – 150.
[19] S. Collins, W. M. Kelly, D. A. Holden, *Macromolecules* **1992**, *25*, 1780 – 1785.
[20] M. Jezequel, V. Dufaud, M. J. Ruiz-Garcia, F. Carrillo-Hermosilla, U. Neugebauer, G. P. Niccolai, F. Lefebvre, F. Bayard, J. Corker, S. Fiddy, et al., *J. Am. Chem. Soc.* **2001**, *123*, 3520 – 3540.
[21] E. Parry, *J. Catal.* **1963**, *2*, 371 – 379.
[22] C. Morterra, G. Cerrato, *Langmuir* **1990**, *6*, 1810 – 1812.
[23] E. P. Talsi, N. V. Semikolenova, V. N. Panchenko, A. P. Sobolev, D. E. Babushkin, A. A. Shubin, V. A. Zakharov, *J. Mol. Catal. A* **1999**, *139*, 131 – 137.
[24] L. L. Böhm, *Angew. Chem. Int. Ed.* **2003**, *42*, 5010 – 5030; *Angew. Chem.* **2003**, *115*, 5162 – 5183.
[25] G. Fink, B. Steinmetz, J. Zechlin, C. Przybyla, B. Tesche, *Chem. Rev.* **2000**, *100*, 1377 – 1390.
[26] A. Alexiadis, C. Andes, D. Ferrari, F. Korber, K. Hauschild, M. Bochmann, G. Fink, *Macromol. Mater. Eng.* **2004**, *289*, 457 – 466.

Manuscript received: April 7, 2018
Accepted manuscript online: May 7, 2018
Version of record online: June 8, 2018